3208–3215 *Nucleic Acids Research, 1996, Vol. 24, No. 16*

The DNA supercoiling architecture induced by the transcription factor xUBF requires three of its five HMG-boxes

V. Y. Stefanovsky, D. P. Bazett-Jones[1], G. Pelletier and T. Moss*

Departement de Biochimie et Centre de Recherche en Cancérologie de l'Université Laval (CRCUL), Hôtel-Dieu de Québec, 11 Côte du Palais, Québec G1R 2J6, Canada and [1]Department of Medical Biochemistry and Anatomy, Faculty of Medicine, Health Sciences Center, University of Calgary, Alberta T2N 4N1, Canada

Received April 26, 1996; Revised and Accepted July 2, 1996

ABSTRACT

The formation of a near complete loop of DNA is a striking property of the architectural HMG-box factor xUBF. Here we show that DNA looping only requires a dimer of Nbox13, a C-terminal truncation mutant of xUBF containing just HMG-boxes 1–3. This segment of xUBF corresponds to that minimally required for activation of polymerase I transcription and is sufficient to generate the major characteristics of the footprint given by intact xUBF. Stepwise reduction in the number of HMG-boxes to less than three significantly diminishes DNA bending and provides an estimate of bend angle for each HMG-box. Together the data indicate that a 350 ± 16° loop in 142 ± 30 bp of DNA can be induced by binding of the six HMG-boxes in an Nbox13 dimer and that DNA looping is probably achieved by six in-phase bends. The positioning of each HMG-box on the DNA does not predominantly involve DNA sequence recognition and is thus an intrinsic property of xUBF.

INTRODUCTION

Transcription of the ribosomal genes in eukaryotes uses a dedicated polymerase, RNA polymerase I (pol I) and a dedicated set of transcription factors (for recent reviews see 1,2). Probably for this reason, the pol I factors and the promoters they recognize display a high degree of species specificity. Despite this specificity, promotion by pol I appears to be mechanistically similar in mammals and amphibia. The promoter generally consists of two precisely spaced sequence elements, the upstream control element (UCE) and the Core promoter element. These elements have been well-defined by surrogate genetics in several organisms. They do not, however, display significant sequence homology. The major steps in the assembly of a pol I pre-initiation complex are known (3–8). Recognition of the UCE and the Core promoter elements by the so-called upstream binding factor (UBF) allows the entry of a pol I-specific TBP–TAF complex, variously called SL1, TIF-IB, TFID, Factor D or Rib1. This leads to the formation of a stable pre-initiation complex which can be specifically recognized by an activated form of pol I. UBF, therefore, plays a key role in promoter recognition and in pre-initiation complex assembly. Surprisingly, UBF displays little detectable sequence selectivity (9,10). Despite this, UBFs from human, mouse, rat and *Xenopus* recognize pol I promoters in a very similar manner. *Xenopus* UBF (xUBF) does not, however, support the entry of SL1 to the mammalian promoters and the converse also appears to be true (11–15).

The UBFs contain multiple HMG-box DNA binding domains. These domains are a characteristic of a large subgroup of architectural transcription factors (16,17). HMG-boxes are especially known for their capacity to induce severe kinks in their DNA target sequences (18–20). XUBF contains five tandemly arranged homologies to the HMG-box domain (21,22) (Fig. 1A). We have previously shown that xUBF binds to the transcription initiation site of the *Xenopus* pol I promoter such that its HMG-box 1 protects bases –21 to –2 and +2 to +21 and HMG-boxes 2 and 3 protect bases downstream of +22 (23). Using electron spectroscopic imaging (ESI) we have directly measured the stochiometry of single xUBF–DNA complexes, showing them to each contain two xUBF molecules (24). Most strikingly, the binding of a single xUBF dimer to the *Xenopus* ribosomal enhancers induces an Enhancesome complex in which a short segment of DNA is looped in to a near complete turn (24). Together, the footprinting and ESI data strongly suggest that within the Enhancesome two xUBF molecules position themselves head to head along the DNA (Fig. 1A). The manner in which xUBF induces DNA looping and the role of its five tandem HMG-boxes in the process are presently unknown. Ligation-mediated circularization and supercoiling studies have suggested that HMG-box 1 alone may be sufficient (25). However, HMG-boxes 2 and 3 are known to be required to reconstitute the full DNA binding affinity of wild-type (wt) xUBF (23) and to support *in vitro* transcription (15,26). Here we define the minimal protein and DNA requirements for the formation of the Enhancesome.

MATERIALS AND METHODS

Expression and isolation of xUBF mutants

Mutants were assembled in the vector pGEX-2T, expressed in *Escherichia coli* and purified as previously described (23,27). Nbox13 was produced by fusing amino acids 16–383 to the GST,

* To whom correspondence should be addressed

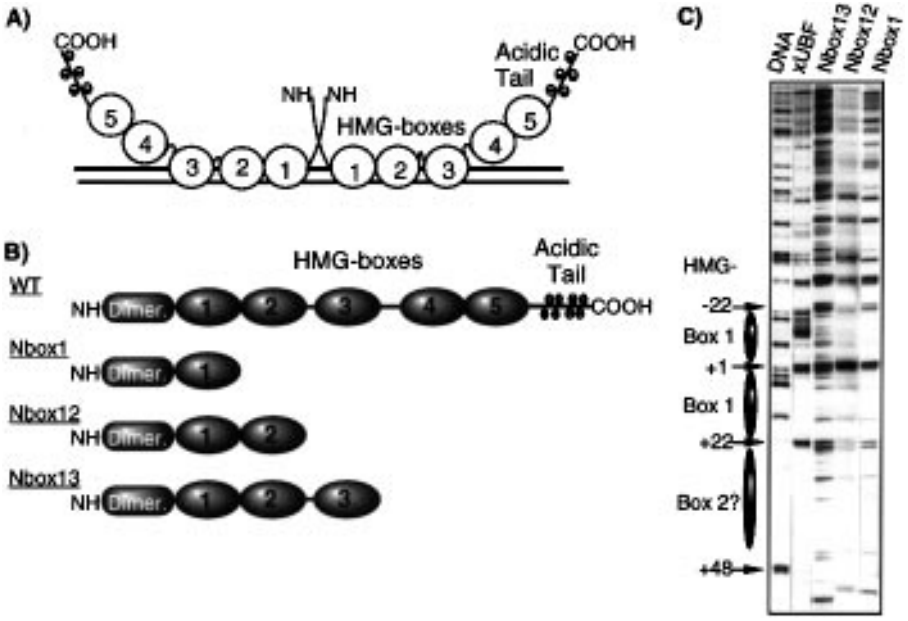

Figure 1. The structure of the xUBF truncation mutants. (**A**) The probable linear arrangement of an xUBF dimer bound to DNA. (**B**) The structure of the three truncation mutants. (**C**) Comparative footprinting of wt xUBF and the truncation mutants across the ribosomal transcription initiation site; 'DNA' refers to unprotected DNA. The footprints due to the various HMG-boxes are indicated, numbers refer to promoter bp relative to initiation at +1.

which was not cleaved from the final product. Box13 (amino acids 101–383) was isolated in the same way, while Nbox1 (amino acids 16–202) and Nbox 12 (amino acids 16–273) were released from the GST domain by thrombin cleavage. The Nbox1 and Nbox12 mutants gave single bands on Tris–Tricine–SDS gels (28). The batches of Nbox13 and Box13 mutants were the same as used in a previous study (23) and showed no change on SDS gel analysis. Protein concentrations were estimated using the appropriate calculated extinction coefficient at 280 nm. Footprinting was performed as previously described (29).

ESI analysis of protein–DNA complexes. Each mutant xUBF (1 µg) was incubated in 25 µl of 50 mM HEPES (pH 7.6), 5 mM $MgCl_2$, 80 mM KCl, 1 mM DTT with 200 ng of the *Xenopus laevis* 1.1 kb *Bam*HI enhancer DNA fragment (30,31) or the 1.046 kb *Pvu*I fragment from pT3T7U19 (Pharmacia). After 15 min at room temperature, the mixture was chromatographed on a 0.5 ml column of Sepharose CL-2B to separate DNA-bound xUBF from free protein. The column buffer contained 10 mM HEPES (pH 7.2), 5 mM $MgCl_2$, 1% formaldehyde, 0.5% glutaraldehyde. The peak DNA fraction (5 µl) was placed on a 1000-mesh copper electron microscope grid, which had been coated with a 3 nm carbon film and glow discharged immediately before use (32). After 30 s, excess sample was washed from the grid with H_2O and the grid air dried after all but a thin layer of the H_2O had been removed.

ESI analysis of DNA–protein complexes has been previously described (32,33). A brief description follows. Estimation of the masses of the xUBF–DNA complexes was carried out on a reference image recorded at 120 eV in the electron energy loss spectrum. DNA was used as an internal mass standard and the mass of the complex was estimated by comparison of integrated optical density of the complex with the integrated optical density over a defined length of DNA. Net phosphorus images were obtained by subtraction of the 120 eV reference image from a 155 eV energy loss image recorded at the peak of the phosphorus L2,3 ionization edge, after alignment and normalization. Results were compared quantitatively with a multiple parameter background correction using two pre-edge images recorded at 105 and 120 eV (see 32). The phosphorus content of the complex was estimated by comparing the integrated phosphorus signal in the complex to that of a defined length of DNA. This value was used to calculate the DNA content in the complex and subtracted from the total mass estimate to obtain the protein content.

RESULTS

To study the HMG-box requirements for the induction of a complete Enhancesome, three truncation mutants of xUBF were produced, each containing an increasing number of HMG-box domains (Fig. 1B). The DNase I footprints of the mutant and wild-type xUBFs were found to be very similar (Fig. 1C). [Those for xUBF, Nbox13 and Nbox1 have been previously described in some detail (23) and are shown here to allow a comparison.] Each showed a clear footprint of ~20 bp immediately upstream and downstream of the *Xenopus* ribosomal RNA initiation site. However, some minor differences in the footprints could be discerned. The two shorter mutants Nbox1 and Nbox12 gave strong hypersensitivity at –1, +1 and protection to either side of this site as far as the hypersensitive sites at –22 and +22, the previously defined boundaries for HMG-box 1 (23). However, these latter sites were especially weak in the case of Nbox12, consistent with the idea that HMG-box 2 may protect bases upstream of –22 and downstream of +22. Wt xUBF and Nbox13 yielded a weaker cleavage at –1, +1 than did Nbox1 and Nbox12, but gave stronger cleavages at the +22 and –22 sites. Thus, HMG-box 2 binding to the regions upstream of –22 and downstream of +22 may be modulated by the addition of HMG-box 3. This may relate to the ESI findings described below.

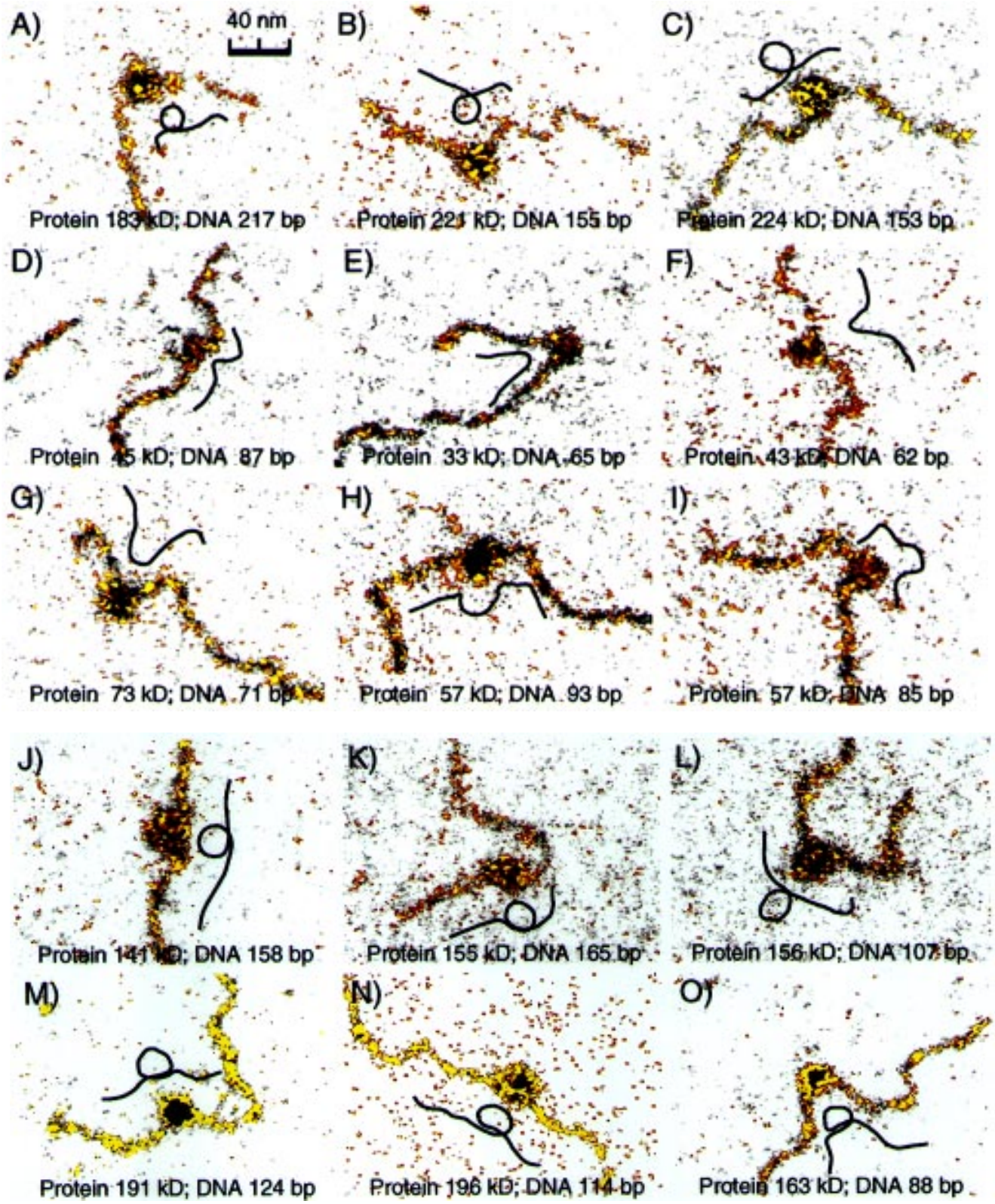

Figure 2. ESI of the xUBF complexes. (**A**–**C**) wt xUBF, (**D**–**F**) Nbox1, (**G**–**I**) Nbox12, (**J**–**O**) Nbox13. (A–L) show complexes on the 1.1 kb *Xenopus* rDNA enhancer repeat, while (M–O) show complexes on a 1.5 kb bacterial DNA fragment (see Materials and Methods). Each image is a superimposition of the total mass image in gray tone and the phosphorous image in a false colour red to yellow spectrum. Protein masses and DNA length for the individual complexes are given and the probable DNA path is indicated adjacent to each complex in black.

Table 1. The numerical data obtained with each of the xUBF truncation mutants are given

Protein-moiety	Protein Species	N	Protein kD Measured	Protein-dimer kD Expected	DNA bp Phosphorous	DNA bp ΔContour	DNA bp Expected ?
xUBF	-	-	217.0 ± 33	210.0	185.0 ± 30	173.0 ± 40	120-127 (200-212)
Nbox1	Dimers	21	35.0 ± 9	40.0	62.0 ± 14		40-42
	All	23	40.0 ± 18		63.0 ± 14		
Nbox12	Dimers	27	61.0 ± 8	63.0	102.0 ± 38		80-85
	All	36	54.0 ± 15		99.0 ± 38		
Nbox13	Dimers	12	155.0 ± 15	147.0	165.0 ± 21	144.0 ± 12 (N=6)	120-127
	All	16	133.0 ± 37	(GST-Nbox13)	164.0 ± 19	142.0 ± 25 (N=10)	
Nbox13-Cntrl DNA	Dimers	8	188.0 ± 35	147.0	122.0 ± 17	121.0 ± 21	120-127
	All	17	167.0 ± 50	(GST-Nbox13)	111.0 ± 26	123.0 ± 28	
All Nbox13	Dimers	20	172.0 ± 32	147.0	142.0 ± 30	129.0 ± 21 (N=14)	120-127
	All	33	150.0 ± 45	(GST-Nbox13)	137.0 ± 35	130.0 ± 28 (N=27)	

Complexes were classified as containing dimers of the protein species when the protein mass was numerically closer to the expected dimer mass than to a monomer or tetramer mass. In the case of Nbox 13, two estimates for the DNA component are given. 'Phosphorous' indicates a mass in bp calculated directly from the net phosphorous image, while the 'Δ Contour' was calculated from the length shortening of the DNA fragment containing a single complex compared with the uncomplexed DNA on the same grid. The 'DNA bp Expected' were calculated assuming a helical repeat of 10–10.6 bp and a two DNA turn repeat for adjacent HMG-box binding sites. 'Nbox 13-Cntrl DNA' refers to complexes on a 1.5 kb bacterial DNA fragment (see Materials and Methods) and 'All Nbox13' to the totality of Nbox 13 images analyzed, regardless of the DNA fragment

[The hypersensitivity around –15, seen only when wt xUBF is bound, has been previously ascribed to the acidic tail of xUBF, which is believed to fold back onto this region (24).]

The first three HMG-boxes of xUBF are sufficient to induce the major characteristics of the Enhancesome

ESI is ideally suited for visualizing DNA–protein complexes since, (i) the specimen does not have to be stained or shadowed, (ii) it allows direct estimation of the mass of complexes and (iii) net phosphorous images localize the DNA component and allow the DNA content to be estimated. Together, the mass information and the phosphorus content can reveal stoichiometric relationships between protein and DNA. We have previously used ESI to resolve the structure of the Enhancesome, showing it to contain a dimer of xUBF and a near complete loop of DNA (24) (see examples in Fig. 2A–C). Therefore, we again used ESI to compare the DNA–protein structures formed by each of the xUBF mutants.

When the smallest mutant, Nbox1, was bound to the ribosomal enhancer DNA, distinct complexes were seen (Fig. 2D–F). The mass distribution of both the DNA and protein components of these complexes is shown in Figure 3 and summarized in Table 1. They show that the great majority of complexes contained a dimer of Nbox1 (35 ± 9 kDa) and 62 ± 14 bp of DNA, only a little longer than the 40–44 bp we would expect from footprint data. The Nbox1 complexes were almost all associated with a kink or bend in the DNA. A similar experiment with Nbox12 again gave complexes which were associated with a kink or a bend in the DNA (Fig. 2G–I). The Nbox12 complexes predominantly contained a dimer of the protein moiety (27 of 36; 61 ± 8 kDa) and were associated with 102 ± 38 bp of DNA (Fig. 3 and Table 1). Neither the Nbox12 nor the Nbox1 complexes showed any evidence of the type of DNA looping associated with the Enhancesome. In the case of Nbox1, the complexes also clearly did not contain sufficient DNA to form a loop of a similar size to that observed in the wild type Enhancesome (Fig. 2A–C and Table 1).

When complexes formed with Nbox13 were observed they showed a close resemblance to the Enhancesome (Fig. 2J–L). Most complexes (12 of 16) clearly contained a protein dimer (155 ± 15) and 165 ± 21 bp of DNA (see Fig. 3 and Table 1. This DNA length compares quite favorably with the previous estimates of 185 ± 30 bp of DNA within the Enhancesome. DNA contour length shortening gave a similar estimate of the DNA in the Nbox13 complexes 144 ± 12, again consistent with that for the Enhancesome of 173 ± 40. Further, a full loop of DNA was noted in 50% of the Nbox13 complexes analyzed. The diameter of this loop could be estimated in many cases and was found to lie between 13 and 19 nm, depending on the image and the axis along which the measurement was made (e.g. Fig. 2J–L and M–O; see below). Assuming a circular loop of DNA, this diameter corresponds to 136–173 bp. Thus, its size is consistent with the DNA of the Enhancesome forming a single near 360° loop.

To test the requirement for the N-terminal dimerization domain of xUBF we also attempted to form complexes with Box13 (23), an N-terminal truncation of Nbox13 in which the dimerization domain had been deleted; see Material and Methods. However, we were unable to form distinct complexes with this mutant.

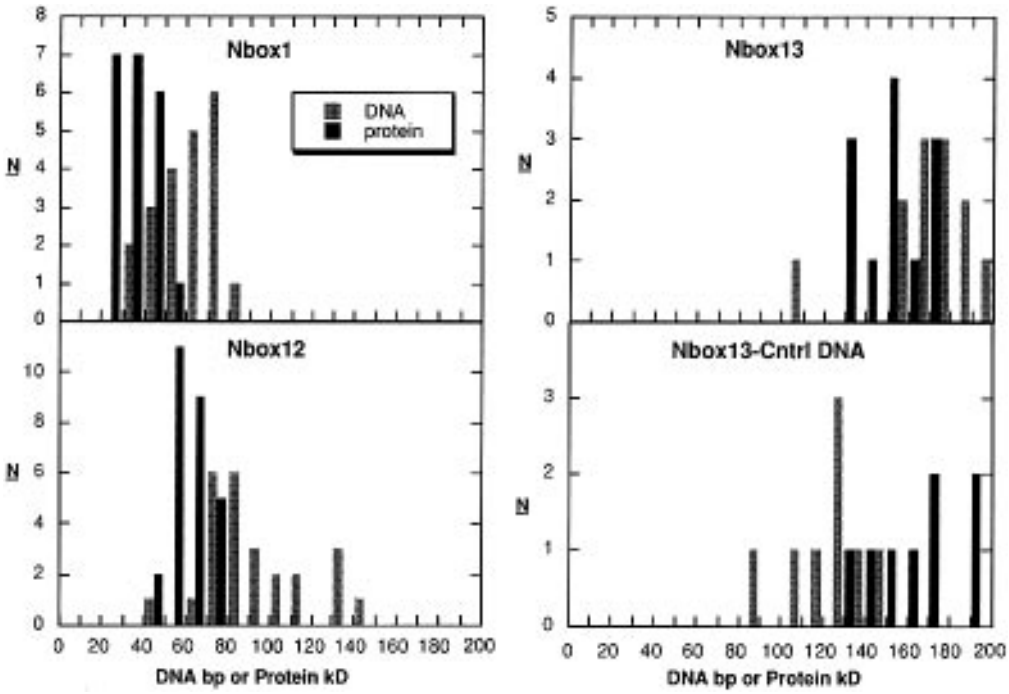

Figure 3. The protein and DNA components of the xUBF–DNA complexes. The raw data for each mutant or DNA is shown in histogram form. 'Cntrl DNA' refers to the 1.5 kb bacterial DNA fragment. Data for the dimer-complexes only (see Table 1) is shown.

DNA-bending induced by HMG-boxes 1 and 3 is the more significant

The Nbox1 and Nbox12 complexes showed clear DNA kinking or bending. Estimates of the degree of kinking could therefore be obtained by measuring the angle between the incoming and outgoing branches of the DNA duplex. These data (Fig. 4), showed a tight distribution of bend angles for both types of complex. In the case of Nbox1, the data gave an average bend angle of 145 ± 24°, i.e., 73 ± 12° for each HMG-box 1. This bend angle is well within the range of 30–130° measured for other HMG-box proteins (18,20). However, addition of HMG-box 2 in the Nbox12 mutant did not appear to greatly increase DNA bending, an average bend of 160 ± 16° being measured for this mutant. This suggests that HMG-box 2 induces only a weak bending of the DNA of somewhere between 0 and 27° (excluding the possibility of negative bend angles).

Bend angle measurements on the Nbox13 complexes (Fig. 4) confirmed that this mutant induced a near complete looping of the DNA (350 ± 16°) clearly distinct from the 145 or 160° bends seen with Nbox1 and Nbox12 respectively. The addition of HMG-box 3 to the complex, therefore, induce a very significant extra DNA bending. The difference between the Nbox12 and Nbox13 bend angles [(350–160)/2] gives an estimate of the bending induced by each HMG-box 3 of the Nbox13 dimer as 95 ± 16°. Again, this figure lies well within the observed range of bend angles induced by HMG-boxes of other factors (18,20). The DNA path defined by the HMG-box 1 to -box 3 bend angles is modeled in Figure 5A. Here, each HMG-box is assumed to induce a distinct bend in the DNA and these bends have been placed at 20 bp intervals, equivalent to about one duplex turn and the approximate footprint of a single HMG-box. Thus, in the model the bends are additive or in-phase. On the basis of this model, the minimum and maximum 'diameters' predicted for the DNA loop of an Enhancesome, 12 and 18 nm respectively, are consistent with the measured range of 13–19 nm estimated from the net phosphate DNA images (Fig. 2J–O).

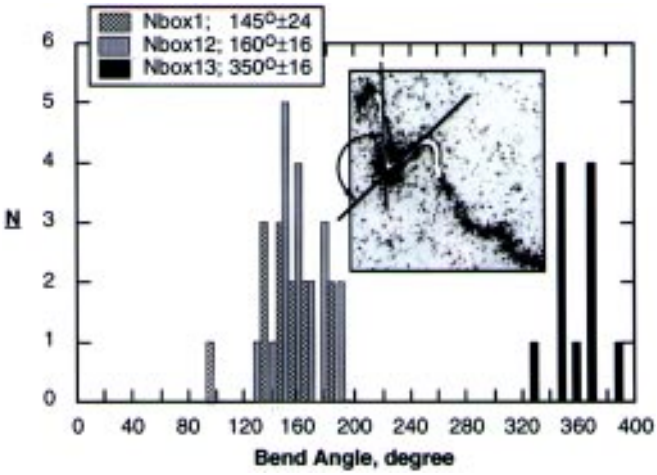

Figure 4. DNA bending by the xUBF mutants. The bend angle was estimated from the phosphorous (DNA) images for each complex essentially as shown in the inset. Here a total mass image is shown for clarity and the DNA path is indicated in white. The mean bend angles and standard deviations for each type of complex are also indicated.

The small degree of apparent bending by HMG-box 2 was somewhat surprising. However, an alternative explanation of our data is possible. It could be envisioned that the binding of HMG-box 3 induces a conformational change in the adjacent box 2, or that boxes 2 and 3 cooperate in some other way to induce a greater bending at box 2 than occurs in the Nbox12 mutant.

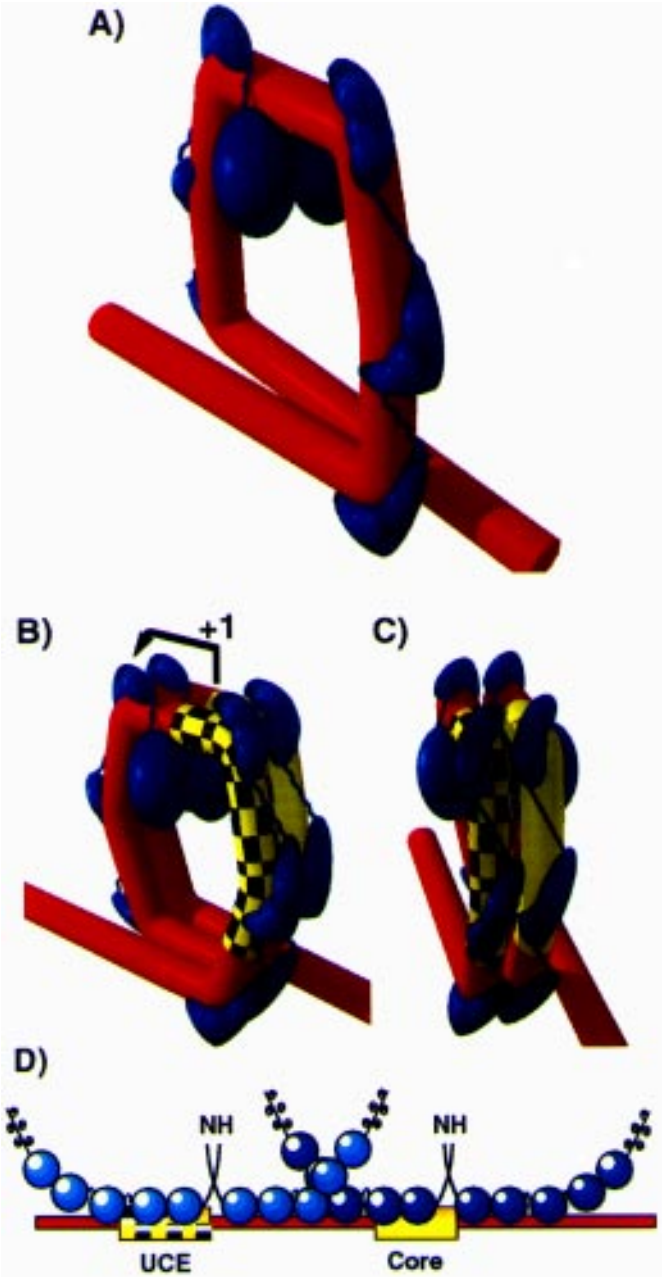

Figure 5. The Enhancesome and a scenario for the structure of the ribosomal promoter. (**A**) An approximate space filling model of the Enhancesome, showing the first three HMG-boxes of xUBF bound at 20 bp repeat around a bent DNA duplex. The DNA has been modeled as a simple cylinder of 2 nm diameter and the HMG-boxes modeled on the HMG-box b of HMG-2 as two interpenetrating ellipsoids and a central sphere. (**B** and **C**) Views of the hypothetical promoter structure. Two Enhancesomes have been placed adjacent to each other such that all HMG-boxes are at 20 bp or two helical turn spacing. The promoter UCE is shown chequered black and yellow, while the Core is shown in yellow and the initiation site indicated +1. (**D**) The probable linear arrangement of UBF on a typical ribosomal promoter.

Footprinting of the xUBF mutants (Fig. 1C) provided some support for the idea of an HMG-box 2/3 cooperativity. On the ribosomal promoter the hypersensitive site flanking HMG-box 1 at +22 bp was clearly evident only in the Nbox13 and wild-type proteins (see Fig. 1C and associated discussion). Direct measurements of the bending due each isolated HMG-boxes may provide more information. However, to date, the poor sequence selection of the HMG-boxes of xUBF, like those of HMG 1 and 2, has, in our hands, prevented the successful application of circular permutation assays (34).

DNA looping is a property intrinsic to xUBF

The DNA bends due to each HMG-box are shown in Figure 5A as being in-phase, i.e., they all lie approximately in the same plane. However, for this to occur the HMG-boxes must be precisely positioned such that they all bind to the same face of the DNA. On B-form DNA, a spacing change of only one base pair between the binding sites of adjacent HMG-boxes would already lead to a change of ~36° between the bends induced by these HMG-boxes. Larger spacing changes would lead to proportionately greater angles. Such spacing changes would, therefore, be observed as very significant pitch changes in the DNA path through the Enhancesome. What then determines the positioning of the HMG-boxes on the target DNA? One possibility is that each HMG-box is directed to its site by DNA sequence preferences. However, it has previously been shown that DNA-binding by xUBF is extremely sequence tolerant (9,10,23). A second possibility is that inter-HMG-box interactions enable the individual HMG-boxes of xUBF to position themselves correctly along the DNA. In this case in-phase bending would be a property intrinsic to xUBF and would occur equally on any DNA fragment, regardless of its sequence.

To decide between these alternatives, Nbox13 was bound to a 1 kb fragment of bacterial DNA and analyzed by ESI in comparison with the enhancer DNA bound complex (Fig. 2M–O). Mass analyses (Fig. 3 and Table 1) (Nbox13–control DNA), showed that nearly 50% of the complexes (8 of 17) contained a protein dimer (188 ± 35 kDa) and 122 ± 17 bp of DNA. Contour length measurements of the DNA confirmed this latter figure (121 ± 21 bp). The complexes on the bacterial DNA showed a somewhat larger dispersion of protein masses than those on the ribosomal enhancer DNA, suggesting that their formation may be somewhat impaired. However, they displayed no sequence (data not shown) and >50% showed a clear loop of DNA. The diameter of this loop corresponded closely with that observed on the enhancer DNA (Fig. 2J–L). Thus, it would appear that the formation of an Enhancesome is at least in greater part independent of DNA sequence.

DISCUSSION

The formation of the Enhancesome complex, in which DNA is folded into a near 360° loop, is the very striking property of the polymerase I transcription factor xUBF (24). Here we have mapped the minimal protein domains required for this Enhancesome structure. The data characterize the Enhancesome as containing a dimer of xUBF and 142 ± 30 bp of DNA wound into a single 350 ± 16° DNA turn of 16 ± 3 nm diameter. Formation of the structure minimally requires a dimer of Nbox13, a C-terminal truncation mutant of xUBF containing only HMG-boxes 1–3 and the N-terminal dimerization domain (see Fig. 1A). This segment of xUBF corresponds to that minimally required for activation of polymerase I transcription (15,26). (Attempts to form complexes with a similar mutant in which this N-terminal dimerization domain was deleted were unsuccessful.) Reduction in the number

of HMG-boxes past 3 very significantly reduced the degree of DNA bending. A dimer of the C-terminal truncation mutant Nbox1, containing only the N-terminal most HMG-box 1, induced a DNA kink of 145 ± 24°, while a dimer of Nbox12, containing HMG-boxes 1 and 2 bent the DNA by 160 ± 16°. Together the data suggest that each of the first three HMG-boxes of xUBF induces an independent kink in the DNA and that these kinks are phased in such a way as to be additive, i.e., they induce in-phase bending. Consistent with this, footprinting data have shown that the two HMG-box 1s of an xUBF dimer bind to adjacent 20 bp segments of DNA and that HMG-boxes 2 and 3 most probably occupy adjacent DNA sites [e.g. see Fig. 1A and C and (23)]. Combining this information with the bend angles estimated for each HMG-box, the probable DNA path through the Enhancesome could be modeled (Fig. 5A). This path is consistent with the dimensions of the Enhancesome.

Strong data exists suggesting that HMG-box domains bind the minor DNA groove and lie on the outside of the DNA kink they induce (19,20,35). Hence, it is highly likely that the HMG-boxes of xUBF also bind around the outside of each DNA kink. The Enhancesome therefore probably resembles the structure modeled in Figure 5A. Here, the six HMG-boxes of an Nbox13 dimer are shown bound around the outside of the Enhancesome DNA loop. The model demonstrates the open nature of the Enhancesome and it is evident that no protein–protein contacts could occur across the centre of the loop. This emphasizes the extent to which the Enhancesome structure may rely on in-phase bending for its formation.

Bending by HMG-box 2 was found to be very small compared with that estimated for either HMG-boxes 1 or 3 (box 1, 72± 12°; box 2, 0–27°; box 3, 95 ± 16°). Our data, however, leave open the possibility that HMG-box 3 cooperates with box 2 in inducing full DNA looping. That is, within the Enhancesome the bend angles per box may be more nearly equivalent. Cooperativity between HMG-boxes could be exterted along the DNA duplex. However, the juxtaposition of the two HMG-box 3s within our model (Fig. 5A) suggests that cooperativity might also occur via an interaction between these boxes. That is via a clamping of the two ends of the DNA loop.

The exact positioning of each HMG-box along the DNA would appear to be a prerequisite for the formation of the Enhancesome. However, xUBF and its individual HMG-boxes show little preference for any particular DNA sequence (9,10,23). When Nbox13 was bound on a randomly chosen bacterial DNA fragment, characteristic Enhancesome complexes could be observed by ESI. Thus, at the resolution of this technique, the HMG-boxes of the Nbox13 mutant are able to correctly position themselves on DNA independent of its sequence. The model in Figure 5A suggests that positioning could probably not result from direct contacts between HMG-box domains and may, therefore, be due to a tethering effect of the short intra-domain 'linker' peptide sequences.

UBF is known to permit the binding of the TBP-complex, SL1, to the UCE and Core elements of the polymerase I promoter (3,4,7). What may then be the significance of the Enhancesome structure? The Nbox13 segment of xUBF, shown here to be sufficient for Enhancesome formation, displays the full DNA binding affinity of xUBF (23). It also corresponds with the segment minimally required for *in vitro* transcription in *Xenopus* extracts (26). Data from human and *Xenopus* suggest that two distinct UBF dimers bind within the polymerase I promoter. One of these dimers is associated with the UCE (15) and the other with the Core promoter element (23). A probable scenario for the arrangement of UBF binding along a stereotypical vertebrate pol I promoter is shown in Figure 5D. This arrangement of UBF would lead to the formation of two adjacent Enhancesome structures within the promoter (Fig. 5B and C). The resulting juxtaposition of the UCE and Core elements could then provide a surface for the cooperative binding of a single or two interacting SL1 complexes to these two promoter elements. This model also provides an explanation of the requirement for stereo-specific alignment of the UCE and Core elements observed for the mammalian, amphibian and even possibly the yeast polymerase I promoters (36–38). The close resemblance in DNA size, though not number of DNA turns, of the Enhancesome to a chromatin Core nucleosome may also be more than a coincidence. It is known that the *Xenopus* ribosomal enhancer chromatin loses its characteristic micrococcal nuclease ladder on gene activation (39,40) (and unpublished data of Leblanc and Moss). However, it has also been shown that the Core histones remain in contact with the enhancers via their N-terminal tails (41,42). The Enhancesome allows ample space to accommodate the Core histones within the DNA loop. At the same time the diameter of the Enhancesome DNA loop would of necessity prevent normal DNA–protein contacts with the globular Core of the histone octamer.

ACKNOWLEDGEMENTS

We wish to extend our thanks to M. Herfort for his excellent assistance. We also thank Dr C. Read for the generous donation of the xUBF2 pGEX2T subclone of amino acids 110–189 (Box 1), and both Drs C. Read and C. Crane-Robinson for much technical advice and many useful discussions made possible by a NATO collaborative research grant to C.R. and T.M. (no. 890637). This work was supported by grants from the Medical Research Council of Canada (MRC) to T.M. and D.P. B.-J. and the National Cancer Institute with funds from the Canadian Cancer Society to D.P.B.-J. T.M. is an MRC of Canada Scientist and a member of the Centre de Recherche en Cancérologie de l'Université Laval which is supported by the FRSQ of Québec. G.P. is supported by an award from the FCAR-FRSQ of Quebec.

REFERENCES

1 Moss,T. and Stefanovsky,V.Y. (1995) In Cohn,W.E. and Moldave,K. (eds), *Progress in Nucleic Acids and Molecular Biology.* Academic Press, Inc., San Diego, pp. 25–66.
2 Paule,M.R. (1993) *Gene Exp.*, **3**, 1–9.
3 Bell,S.P., Learned,R.M., Jantzen,H.M. and Tjian,R. (1988) *Science*, **241**, 1192–1197.
4 McStay,B., Hu,C.H., Pikaard,C.S. and Reeder,R.H. (1991) *EMBO J.*, **10**, 2297–2303.
5 Schnapp,A., Clos,J., Hädelt,W., Schreck,R., Cvekl,A. and Grummt,I. (1990) *Nucleic Acids Res.*, **18**, 1385–1393.
6 Tanaka,N., Kato,H., Ishikawa,Y., Hisatake,K., Tashiro,K., Kominami,R. and Muramatsu,M. (1990) *J. Biol. Chem.*, **265**, 13836–13842.
7 Smith,S.D., Oriahi,E., Lowe,D., Yang-Yen,H.-F., O'Mahony,D., Rose,K., Chen,K. and Rothblum,L.I. (1990) *Mol. Cell Biol.*, **10**, 3105–3116.
8 Paule,M.R., Bateman,E., Hoffman,L., Iida,C., Imboden,M., Kubaska,W., Kownin,P., Li,H., Lofquist,A., Risi,P., Yang,Q. and Zwick,M. (1991) *Mol. Cell Biochem.*, **104**, 119–126.
9 Copenhaver,G.P., Putnam,C.D., Denton,M.L. and Pikaard,C.S. (1994) *Nucleic Acids Res.*, **22**, 2651–2657.
10 Hu,C.H., McStay,B., Jeong,S.W. and Reeder,R.H. (1994) *Mol. Cell Biol*, **14**, 2871–2882.

11 Bell,S.P., Pikaard,C.S., Reeder,R.H. and Tjian,R. (1989) *Cell*, **59**, 489–497.
12 Pikaard,C.S., McStay,B., Schultz,M.C., Bell,S.P. and Reeder,R.H. (1989) *Genes Dev.*, **3**, 1779–1788.
13 Pikaard,C.S., Smith,S.D., Reeder,R.H. and Rothblum,L. (1990) *Mol. Cell Biol.*, **10**, 3810–3812.
14 Cairns,C. and McStay,B. (1995) *Nucleic Acids Res.*, **23**, 4583–4590.
15 Jantzen,H.M., Chow,A.M., King,D.S. and Tjian,R. (1992) *Genes Dev.*, **6**, 1950–1963.
16 Wolffe,A.P. (1994) *Science*, **264**, 1100–1101.
17 Wickelgren,I. (1995) *Science*, **270**, 1587–1588.
18 Grosschedl,R., Giese,K. and Pagel,J. (1994) *Trends Genet.*, **10**, 94–100.
19 Werner,M.H., Huth,J.R., Gronenborn,A.M. and Clore,G.M. (1995) *Cell*, **81**, 705–714.
20 Read,C.M., Cary,P.D., Crane-Robinson,C., Driscoll,P.C., Carrillo,M.O.M. and Norman,D.G. (1995) In Eckstein,F. and Lilley,D.M.J. (eds), *Nucleic Acids and Molecular Biology, vol 9*. Springer-Verlag, Berlin Heidelberg, pp. 222–250.
21 Bachvarov,D. and Moss,T. (1991) *Nucleic Acids Res.*, **19**, 2331–2335.
22 Bachvarov,D., Normandeau,M. and Moss,T. (1991) *FEBS Lett.*, **288**, 55–59.
23 Leblanc,B., Read,C. and Moss,T. (1993) *EMBO J.*, **12**, 513–525.
24 Bazett-Jones,D.P., Leblanc,B., Herfort,M. and Moss,T. (1994) *Science*, **264**, 1134–1137.
25 Putnam,C.D., Copenhaver,G.P., Denton,M.L. and Pikaard,C.S. (1994) *Mol. Cell Biol*, **14**, 6476–6488.
26 McStay,B., Frazier,M.W. and Reeder,R.H. (1991) *Genes Dev.*, **5**, 1957–1968.
27 Smith,D.B. and Corcoran,L.M. (1991) In Ausubel,F.M., Brent,R., Kingston,R.E., Moore,D.D., Seidman,J.G., Smith,J.A. and Struhl,K. (eds), *Current Protocols in Molecular Biology*. Greene Publishing Associates & Wiley-Interscience, New York.
28 Schagger,H. and von Jagow,G. (1987) *Anal. Biochem.*, **166**, 368–379.
29 Read,C., Larose,A.M., Leblanc,B., Bannister,A.J., Firek,S., Smith,D.R. and Moss,T. (1992) *J. Biol. Chem.*, **267**, 10961–10967.
30 Moss,T. (1983) *Nature*, **302**, 223–228.
31 De Winter,R.F.J. and Moss,T. (1987) *J. Mol. Biol.*, **196**, 813–827.
32 Bazett-Jones,D.P. (1993) *Microbeam Analysis*, **2**, 69–79.
33 Bazett-Jones,D.P. and Brown,M.L. (1988) *Mol. Cell Biol.*, **9**, 336–341.
34 Wu,H.-M. and Crothers,D.M. (1984) *Nature*, **308**, 509–513.
35 Love,J.J., Li,X., Case,D.A., Giese,K., Grosschedl,R. and Wright,P.E. (1995) *Nature*, **376**, 791–795.
36 Xie,W.Q. and Rothblum,L.I. (1992) *Mol. Cell Biol.*, **12**, 1266–1275.
37 Pape,L.K., Windle,J.J. and Sollner-Webb,B. (1990) *Genes Dev.*, **4**, 52–62.
38 Choe,S.Y., Schultz,M.C. and Reeder,R.H. (1992) *Nucleic Acids Res.*, **20**, 279–285.
39 Spadafora,C. and Crippa,M. (1984) *Nucleic Acids Res.*, **12**, 2691–2704.
40 Lucchini,R. and Sogo,J.M. (1992) *Mol. Cell Biol.*, **12**, 4288–4296.
41 Dimitrov,S.I., Stefanovsky,V.Y., Karagyozov,L., Angelov,D. and Pashev,I.G. (1990) *Nucleic Acids Res.*, **18**, 6393–6397.
42 Dimitrov,S.I., Tateossyan,H.N., Stefanovsky,V.Y., Russanova,V.R., Karagyozov,L. and Pashev,I.G. (1992) *Eur. J. Biochem.*, **204**, 977–981.